

Preparation of Long-Term Antibacterial SiO₂-Cinnamaldehyde Microcapsule via Sol-Gel Approach as a Functional Additive for PBAT Film

Authors:

Yangfan Xu, Chongxing Huang, Xiujie Dang, Muhammad Rafiullah Khan, Haohe Huang, Yuan Zhao, Shuangfei Wang

Date Submitted: 2020-11-24

Keywords: composite film, antibacterial materials, PBAT, cinnamaldehyde

Abstract:

The mesoporous silica wall materials can achieve controlled load and sustained-release of active agents. An antimicrobial nanoscale silica microcapsule containing cinnamaldehyde (CA) was prepared by the sol-gel method and applied in poly (butylenedipate-co-terephthalate) (PBAT) film. The surface morphology, physical and chemical properties, and antibacterial properties of microcapsules and films were studied. The effects of different temperatures and humidities on the release behavior of microcapsules were also evaluated. Results showed that CA was successfully encapsulated in silica microcapsule which had a diameter of 450-700 nm. The antibacterial CA agent had a long-lasting release time under lower temperature and relative humidity (RH) environment. At low temperature (4 °C), the microcapsules released CA 32.35% in the first 18 h, and then slowly released to 56.08% in 216 h; however, the microcapsules released more than 70% in 18 h at 40 °C. At low humidity (50%RH), the release rates of microcapsules at the 18th h and 9th d were 43.04% and 78.01%, respectively, while it reached to equilibrium state at 72 h under 90% RH. The sustained release process of CA in SiO₂-CA microcapsules follows a first-order kinetic model. Physicochemical properties of PBAT films loaded with different amounts of microcapsules were also characterized. Results showed that the tensile strength and water vapor transmission rate (WVTR) of the composite film containing 2.5% microcapsules were increased by 26.98% and 14.61%, respectively, compared to the raw film, while the light transmittance was slightly reduced. The crystallinity of the film was improved and can be kept stable up to 384.1 °C. Furthermore, microcapsules and composite film both exhibited distinctive antibacterial effect on Escherichia coli and Listeria monocytogenes. Therefore, SiO₂-CA microcapsules and composite films could be a promising material for the active packaging.

Record Type: Published Article

Submitted To: LAPSE (Living Archive for Process Systems Engineering)

Citation (overall record, always the latest version):

LAPSE:2020.1171

Citation (this specific file, latest version):

LAPSE:2020.1171-1

Citation (this specific file, this version):



LAPSE:2020.1171-1v1

DOI of Published Version: <https://doi.org/10.3390/pr8080897>

License: Creative Commons Attribution 4.0 International (CC BY 4.0)

Article

Preparation of Long-Term Antibacterial SiO₂-Cinnamaldehyde Microcapsule via Sol-Gel Approach as a Functional Additive for PBAT Film

Yangfan Xu ¹, Chongxing Huang ^{1,2,*} , Xiujie Dang ¹, Muhammad Rafiullah Khan ¹, Haohe Huang ¹ , Yuan Zhao ^{1,2} and Shuangfei Wang ^{1,2,*}

¹ School of Light Industry and Food Engineering, Guangxi University, Nanning 530004, China; xyflower23@163.com (Y.X.); xiujied@163.com (X.D.); khan87@gxu.edu.cn (M.R.K.); huanghaohe@st.gxu.edu.cn (H.H.); zy199113@163.com (Y.Z.)

² Guangxi Key Laboratory of Clean Pulp & Papermaking and Pollution Control, Nanning 530004, China

* Correspondence: huangcx@gxu.edu.cn (C.H.); wangsf@gxu.edu.cn (S.W.); Tel.: +86-771-327-2256 (C.H.)

Received: 7 July 2020; Accepted: 23 July 2020; Published: 27 July 2020



Abstract: The mesoporous silica wall materials can achieve controlled load and sustained-release of active agents. An antimicrobial nanoscale silica microcapsule containing cinnamaldehyde (CA) was prepared by the sol-gel method and applied in poly (butyleneadipate-*co*-terephthalate) (PBAT) film. The surface morphology, physical and chemical properties, and antibacterial properties of microcapsules and films were studied. The effects of different temperatures and humidities on the release behavior of microcapsules were also evaluated. Results showed that CA was successfully encapsulated in silica microcapsule which had a diameter of 450–700 nm. The antibacterial CA agent had a long-lasting release time under lower temperature and relative humidity (RH) environment. At low temperature (4 °C), the microcapsules released CA 32.35% in the first 18 h, and then slowly released to 56.08% in 216 h; however, the microcapsules released more than 70% in 18 h at 40 °C. At low humidity (50%RH), the release rates of microcapsules at the 18th h and 9th d were 43.04% and 78.01%, respectively, while it reached to equilibrium state at 72 h under 90% RH. The sustained release process of CA in SiO₂-CA microcapsules follows a first-order kinetic model. Physicochemical properties of PBAT films loaded with different amounts of microcapsules were also characterized. Results showed that the tensile strength and water vapor transmission rate (WVTR) of the composite film containing 2.5% microcapsules were increased by 26.98% and 14.61%, respectively, compared to the raw film, while the light transmittance was slightly reduced. The crystallinity of the film was improved and can be kept stable up to 384.1 °C. Furthermore, microcapsules and composite film both exhibited distinctive antibacterial effect on *Escherichia coli* and *Listeria monocytogenes*. Therefore, SiO₂-CA microcapsules and composite films could be a promising material for the active packaging.

Keywords: cinnamaldehyde; PBAT; antibacterial materials; composite film

1. Introduction

Antibacterial packaging is the last line of defense to ensure food safety, representing an active packaging system containing antibacterial substances which can be incorporated into the substrate material either physical or chemical approach [1–3]. Active agents can destroy the structural integrity of cells, prolong the spore dormancy period, or slow down the growth of microorganisms, thereby killing or inhibiting spoilage bacteria and pathogenic bacteria [4]. Plant extracts are extremely effective antibacterial agents extensively applied in food preservation and is favored by consumers due to its natural source and non-toxic qualities [5,6]. Among them, cinnamaldehyde (CA) is well known for

its insecticidal, anti-inflammatory, and anti-tumor effects, which consequently makes it a candidate for active packaging to achieve high-efficiency bacteriostasis even when not in direct contact with microbes [6,7]. It has been approved by the FDA as a food additive, which can inhibit more than 20 common bacteria that could cause human infectious diseases and food breakdown [8]. Uzunlu et al. [9] developed a Polycaprolactone film incorporated CA and observed the antibacterial behavior, studied the release behavior of CA, and found that the release amount exceeded 80% at 21 h which was attributed to the instability of CA. The poor water solubility, and its high susceptibility to degradation by light, heat, oxygen, or free radicals, limits the application of CA in packaging and other fields [10].

The microcapsule technology can ensure the stability of the encapsulated material; for example, Lisuzzo et al. [11] prepared new biohybrid materials based on halloysite nanotubes and natural polymers (alginate and chitosan) for the controlled and sustained release of sodium diclofenac under human gastro-intestinal conditions. Meanwhile, the microcapsules made by the sol-gel method can further avoid the excessive release of the core material, prolong the release time, and achieve the enduring antibacterial purpose, based on the ion diffusion mechanism of the structure [12]. The sol-gel method is a silicon-based material encapsulation technology, while the inorganic wall materials have higher temperature and chemical resistance than organic ones. Valltet-Regi [13] first loaded the hydrophobic drug ibuprofen on the drug carrier of mesoporous silica in 2001, and found that mesoporous silica can prolong the drug release time. Subsequently, more and more researchers turned their attention to the drug-loading function of silica. Xue et al. [14] prepared a hybrid material of polylactic acid-glycolic acid copolymer/mesoporous silica, and the mesoporous silica enabled the sustained release of the loaded gentamicin for more than 20 days. Shane et al. [15] used the emulsion template method to synthesize silica microcapsules, and found that adding a small amount of the silica precursor tetraethyl orthosilicate (TEOS) multiple times was more conducive to achieving sustained-release of the microcapsules. The uniform pore size of mesoporous silica makes it a highly efficient carrier; this is because its high pore volume enables high drug loading and entrapping [16]. In addition, its large specific surface area increases its drug-molecule adsorption capacity [17].

Poly (butyleneadipate-*co*-terephthalate) (PBAT) has emerged as a promising alternative to food packaging materials. It is a novel bio-compostable aliphatic-aromatic polyester obtained from fossil resources by polycondensation and transesterification of poly (butylene adipate) and poly (butylene terephthalate) that combines the advantages of both aliphatic and aromatic polyesters. In other words, it possesses the flexibility and biodegradability of aliphatic polyesters and the good mechanical properties of aromatic polyesters [18–21]. Several researchers have studied that the addition of natural substances can enhance the basic properties of PBAT films and impart antibacterial properties [22,23]. However, no research work has been found on development of antimicrobial nanoscale silica microcapsule containing cinnamaldehyde (CA) and its application in packaging films.

Therefore, this work aimed to develop a formulation to achieve the release of biological control agents triggered by temperature and moisture, so as to achieve sustained-release of CA and long-term antibacterial purposes. Herein, the mesoporous silica wall material was prepared by sol-gel method and used to encapsulate unstable CA to obtain nanoscale antimicrobial microcapsules, and the effect of CA concentration on the encapsulation efficiency was studied. In addition, release study was also conducted at 4, 25 and 40 °C, and 50%, 70%, and 90% relative humidity (RH) to determine the effect of temperature or humidity on the release rate and efficiency. Based on several typical drug release models, CA is used as a model drug to study the release characteristics of microcapsules. Furthermore, microcapsules with different contents were further loaded on the PBAT film to confer antibacterial properties, and the physical and chemical modification effects of the microcapsules on the film were also studied.

2. Materials and Methods

2.1. Materials and Regents

Tetraethyl orthosilicate (TEOS) was purchased from Jinshan Chemical Reagent Co. Ltd. (Chengdu, China). Ammonia (25%) was supplied by Zhiyuan Chemical Reagent Co. Ltd. (Tianjin, China). Cetyl-trimethyl ammonium bromide (CTAB) was procured from Da Mao Chemical Reagent Factory (Tianjin, China). Cinnamaldehyde (CA, $\geq 95\%$) and dimethyl sulfoxide (DMSO) were purchased from Aladdin Reagent Co. Ltd. (Shanghai, China). PBAT (C1200) was supplied by BASF Corporation (Germany). Dichloromethane was obtained from Beichen Founder Reagent Factory (Tianjin, China). All the reagents were of analytical grade.

2.2. Preparation and Characterization of Microcapsules

2.2.1. Preparation of Microcapsules

Microcapsules were prepared by combined sol-gel and oil-in-water techniques. Distilled water was mixed with 0.09 g of surfactant (CTAB) at 25 °C; to this solution, the amount of CA (weight ratios of TEOS to CA of 10:1, 5:1, 5:2, and 5:3) was added and stirred for 30 min to obtain an emulsion. Later, a mixed solution of 95% anhydrous ethanol (59% of water volume) and 0.7 mL TEOS was added dropwise to the emulsion obtained in the first step while stirring and 1.5 mL of ammonia (as a catalyst) was immediately added to accelerate the hydrolysis-condensation reaction of TEOS. The reaction was allowed to continue for 3 h at the stirring speed of 700 revolution/min to obtain SiO₂-CA microcapsule emulsion. The prepared emulsion was centrifuged and washed successively with 95% ethanol and distilled water. Finally, the precipitate was vacuum lyophilized for 15 h.

2.2.2. Characterizations of Microcapsules

Ultraviolet-visible (UV-Vis) absorption spectra of prepared microcapsules supernatants were recorded by UV-Vis spectrophotometry (SPECORD plus 50, Jena Analytical Instruments AG, Germany) over wavelengths ranging from 200 to 500 nm [24]. IR spectra of microcapsules were acquired using FTIR (VERTEX 70, Bruker, Germany) with a buckled KBr sheet in the spectral range of 400 to 4000 cm⁻¹; an average of 32 scans were recorded at a resolution of 4 cm⁻¹. The crystallization was tested on X-ray Diffractometer (XRD, Rigaku MiniFlex600, Japan) using a Cu K α radiation ($\lambda = 0.154$ nm) in the 2θ range 10–40° at room temperature. The surface morphologies of samples were observed using a Field-Emission Scanning Electron Microscope (FE-SEM, Hitachi, Japan) operating at an accelerating voltage of 15 kV. Transmission electron microscopy (TEM) (HT7700, Hitachi High-Tech, Japan) was conducted on the microcapsules at a voltage of 80 kV with commercial copper grids. An surface porosity measurement system (ASAP 2460, McMurray Instruments Co., Ltd., USA) was used to construct the nitrogen adsorption-desorption isotherms of the prepared microcapsules at -195.85 °C. The samples were pretreated in vacuum at 100 °C for 12 h before measurement to remove any impurities and volatiles. The pore-size distribution was calculated from the nitrogen adsorption curve according to the Barrett-Joyner-Halenda method [25].

2.2.3. Encapsulation Efficiency

According to a previous report, the absorbance of CA was measured by UV-Vis spectrophotometry. The active-agent encapsulation efficiency was determined by the following equation [26]:

$$EE = \frac{(M_a - CV)}{M_a} \times 100$$

where *EE* is the encapsulation efficiency, %; *M_a* represents the total amount of CA added; *C* represents the concentration of CA not entrapped in the supernatant of tested liquid; and *V* is the volume of the supernatant.

2.2.4. Sustained-Release Performance of Microcapsules

Active-agent release from the microcapsules was tested according to a modified version of the protocol suggested by Wu et al. [27] and Li et al. [28]. This analysis is mainly focused on the effects of temperature and humidity. SiO₂-CA microcapsules (0.17 g) were incubated at varying temperatures of 4, 23, and 40 °C while maintaining the RH of 90%, and evaluated the release rate at intervals of time (3 h, 6 h, 12 h, 18 h, 24 h, 36 h, 48 h, 3 d, 4 d, 5 d, 7 d, 9 d, 12 d, and 15 d). Each sample was analyzed thrice to reduce measurement error. Similar to the study on the effect of temperature, the RH was varied at 50%, 70%, and 90% while keeping the temperature constant (40 °C). The active-agent release rate was calculated using the following equation:

$$CR = \frac{(1 - M_t)}{M_0} \times 100$$

where *CR* represents the release rate of CA (%), *M_t* is the content of CA in SiO₂-CA microcapsules which is estimated by UV-Vis spectrophotometry method described in the previous section, and *M₀* represents the content of CA in the initial SiO₂-CA microcapsules.

2.2.5. Antibacterial Assay of Microcapsules

E. coli and *Listeria monocytogenes* were used to detect the antimicrobial properties of microcapsules. *E. coli* and *Listeria monocytogenes* strains were purchased from China General Microbiological Culture Collection Center and isolated from our laboratory in Guangxi, China.

This antibacterial activity was determined following a reported disk diffusion method of Moghimi et al. [29]. DMSO (5 mL) was mixed with 40, 50, 60, 70, 80, or 90 mg·mL⁻¹ of SiO₂-CA microcapsules, then dropped the mixed solution (20 μL) on a filter paper with a diameter of 10 mm. A glass Petri dish (150 mm diameter) containing the agar medium was prepared and poured evenly with 100 μL of bacterial suspension containing 10⁷ CFU·mL⁻¹ and then dried for 5 min in a biological safety cabinet. Subsequently, the sterile filter paper samples loaded with antibacterial microcapsules were held at the center of the coated agar plate for 10 min using sterilized tweezers. Finally, the experimental Petri dishes were inverted and cultured in a constant temperature and humidity incubator at 37 °C and 70% RH for 24 h, then the diameter of microorganism-growth-inhibition zones (mm) around the antibacterial filter was measured.

2.3. Preparation and Characterization of Microcapsules Loaded Films

2.3.1. Preparation of Films

According to existing laboratory technology, at room temperature, the ratio of PBAT to dichloromethane is 1 g: 6 mL, mixed for 1 hour, and magnetically stirred for 2 hours to obtain a uniformly mixed film-forming solution. In addition, the dry weight of PBAT SiO₂-CA microcapsules was weighed 0.5%, 2.5%, 4.5%, respectively, slowly added to the uniformly formed film-forming solution, and magnetically stirred until the mixture was uniform (about 2 h). Coating machine (ZAA2300, Zehntner, Swiss) was used to prepare the anti-foam film-forming liquid into a PBAT/SiO₂-CA (PSC) composite antibacterial film. The average thickness of the composite film was recorded as 30 ± 2.50 μm.

For ease of description, herein, 0.5%, 2.5% and 4.5% of the SiO₂-CA microcapsules antimicrobial film are expressed as PSC-0.5%, PSC-2.5% and PSC-4.5%, respectively.

2.3.2. Characterization of Films

SEM: Scanning electron microscope (SEM, Feiner World Pro, FEI company, USA) was used to observe the morphology of the film. The films were brittlely broken in liquid nitrogen and treated with gold spray. under 5.0 kV.

DSC: Differential scanning calorimetry (DSC, Netzsch, Germany) was used to characterize the phase transition and crystallization behavior, the experiment was carried out based on the method of Zhang et al. [30]. The temperature is rapidly increased from room temperature to 180 °C, and the temperature is kept for 10 min to eliminate the thermal history; then, the temperature is reduced to 15 °C at a rate of 10 °C/min and the cooling curve is recorded: increase the temperature to 180 °C at the same heating rate and record the second heating curve. Each sample was analyzed thrice and the average result was reported.

The crystallinity of the pure PBAT and PSC film is calculated as following:

$$X_c = \frac{\Delta H_m}{W_{PBAT}\Delta H_m^0} \times 100\%$$

where, X_c is the crystallinity of the film, %; ΔH_m indicates the melting enthalpy of the film, J/g; is the melting heat enthalpy of the pure PBAT film at 100% crystallization, which was taken as 114 J/g; W_{PBAT} is the weight percentage of PBAT in the PSC film.

TGA: Thermogravimetric Analyzer (TGA, STA449F5, Germany) was used to characterize the thermal stability of the microcapsule antimicrobial films, the experiment conducted the method of Huang et al. [31]. The samples were placed in a crucible, and thermal analysis was performed under nitrogen atmosphere in a temperature range of 20–600 °C at a heating rate of 10 °C/min.

Mechanical properties: According to the ASTM D882-12 test method, 15 × 150 mm² samples were prepared and the longitudinal tensile strength and elongation at break were measured on a universal material testing machine (INSTRON 3367, USA) at a test speed of 100 mm min⁻¹ with an initial pitch of 100 mm. The experiments were performed in triplicate (three replicates, with five film strips per replicate) for films.

Water Vapor Transmission Rates (WVTR): The WVTR of films were measured according to ASTM F1249 using a water vapor transmission instrument (LanGuang, China) at a test temperature of 38 °C and a relative humidity of 90% with a test area of 63.58 cm² for three parallel of each sample. The unit of water vapor transmission rate is g·m⁻²·24·h⁻¹.

Transmittance: Strip samples of 3 × 1 cm² were cut from PBAT and PSC films. Film transmittance was measured using a UV/vis spectrophotometer at a wavelength range of 400–700 nm. Each sample was analyzed thrice and the average result was reported.

2.3.3. Antibacterial Assay of Films

The experimental bacterial inoculum is the same as in Section 2.2.5. This antibacterial activity was based on Li et al. [28], with slight modifications. A total of 0.1 g of the shredded pure PBAT film and PSC composite antibacterial film were mixed with 5 mL of *E. coli* and *Listeria monocytogenes* (10³ and 10² CFU·mL⁻¹) and incubated at 250 rpm and 37 °C for 4 h. After shaking, 0.1 mL of the suspension was removed and cultured on agar medium at 37 °C for 24 h, and the number of viable cells was counted and the inhibition rate was calculated using the following equation:

$$R = 100 \times \frac{(A - B)}{A}$$

where stands for the antimicrobial efficiency (%); is the total number of bacteria; and is the number of bacteria colonies on the PSC film.

2.4. Statistical Analysis

The experimental results are based on the mean ± standard deviation (SD) obtained from the triplicate test. Statistical correlations were evaluated using Pearson's correlation coefficients, and the criterion for significance was $p < 0.05$. Figures were drawn by Origin 8.5 (OriginLab Corp., Northampton, MA, USA).

3. Results and Discussion

3.1. Preparation of Microcapsules

3.1.1. Preparation

The SiO₂-CA microcapsules were prepared by the sol-gel process coupled with oil-in-water method. The synthesis diagram is shown in Figure 1. TEOS, CA, CTAB, ammonia, deionized water and ethanol were mixed, emulsified, and dispersed. CA and TEOS acted as separate oil phases, water and ethanol formed an aqueous phase, and emulsifier CTAB was used as a stabilizer and a removable template. When the silane precursor and catalyst ammonia were dripped into the system, the silane precursor underwent hydrolysis and condensation reactions took place to form a negatively charged organic modified silica oligomer and silanol, and migrated to the positively charged CTAB through electrostatic action. Thus, a complete SiO₂ wall material was continuously deposited on the CA surface.

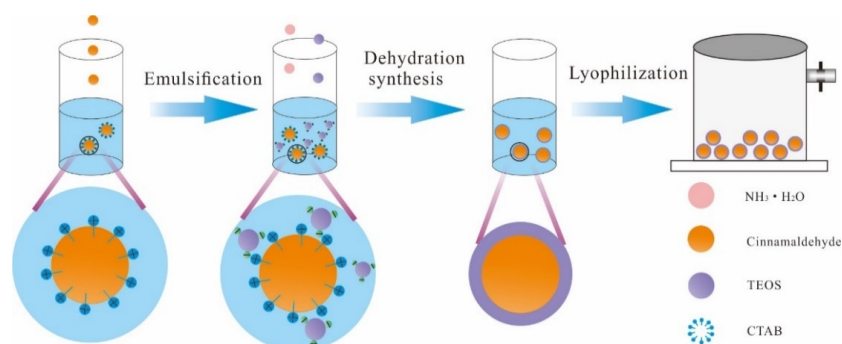


Figure 1. Schematic illustration for the synthesis of SiO₂-CA microcapsules.

3.1.2. Effect of CA Concentration on Encapsulation Efficiency

Figure 2 shows the effect of different CA contents on the encapsulation efficiency of SiO₂-CA microcapsules. When the ratio of TEOS-CA (*v/v*) was 10:1-5:3, the encapsulation efficiency of SiO₂-CA microcapsules first increased and then gradually decreased. Encapsulation efficiency reached to its maximum ($57.64 \pm 0.89\%$) at the TEOS-CA (*v/v*) ratio of 5:1. The reduction rate of TEOS-CA (*v/v*) between 5:1 and 5:2 was less than the reduction rate between 5:2-5:3. This was probably due to the small amount of CA been added. However, when the concentration of the CA increased, the encapsulation efficiency decreased due to the prevention of the CA by silica to form capsules. Interestingly, the encapsulation efficiency also greatly decreased at faster rate where some the free CA molecules were found in the external solution. It is worth noting that when TEOS-CA (*v/v*) was 5:1, the optimal ratio of silica and CA in the system was achieved, and most core materials were wrapped in silica to obtain the most ideal encapsulation efficiency.

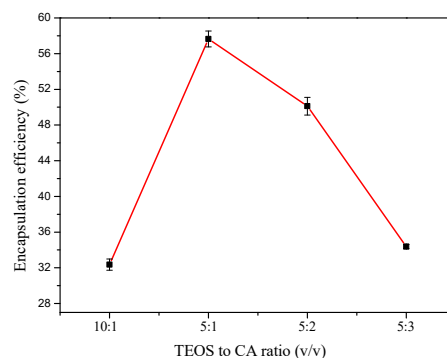


Figure 2. Effect of CA concentrations on the encapsulation efficiency.

The content of CA can be measured indirectly and reliably by UV-Vis spectrophotometry. CA-ethanol solution gives maximum absorption at 278 nm, which is very close to the wavelength reported by Alarcon-Moyano et al. [32]; therefore, we used this wavelength in our study.

3.2. Structural and Morphological Properties of Microcapsules

3.2.1. Functional Structure

Figure 3 shows the Fourier transform infrared spectroscopy (FTIR) spectra of different samples. Curve *a* represents the FTIR spectrum of pure CA. The two weak bands at 2820 and 2742 cm^{-1} could be attributed to the C-H units in CA while the stretching vibration peak at 1682 cm^{-1} could be attributed to aldehydic C=O bonds. The characteristic band at 1631 cm^{-1} was ascribed to C-C stretching in the unsaturated benzene rings and the peaks at 1500 to 1000 cm^{-1} and 970 to 687 cm^{-1} were mainly associated to C-H bending in the aromatic ring [33,34]. In curve *b*, the peaks at 2916 and 2850 cm^{-1} corresponded to CH_2 symmetric stretching vibrations and CH_3 antisymmetric stretching in CTAB, respectively [35]. The spectrum in curve *c* represents blank microcapsules; the stretching and bending vibration peaks corresponding to silicon-hydroxyl groups (Si-OH) formed by the precursor TEOS during hydrolysis and were located at 3396 and 958 cm^{-1} , respectively. The peaks at 455, 788, and 1070 cm^{-1} were attributed to the bending, symmetric stretching, and asymmetric stretching of silicon-oxygen bonds (Si-O-Si) formed by Si-OH, which were similar with the work of Corradini et al. [36]. Curve *d* shows the infrared spectrum of SiO_2 -CA microcapsules. The peaks at 1552 and 1682 cm^{-1} were assigned to C-C bonds and aldehydic C=O bonds, respectively, in unsaturated benzene ring in CA; peaks corresponding to C-H bonds in the aldehyde group (at 2853 and 2920 cm^{-1}) overlapped with the absorption peak of C-H bonds in CTAB. The stretching vibration peaks of C-H in SiO_2 -CA microcapsules were stronger than those of blank microcapsules. The characteristic peak of CA in the FTIR spectrum of SiO_2 -CA microcapsules, confirmed that CA was successfully entrapped in SiO_2 walls.

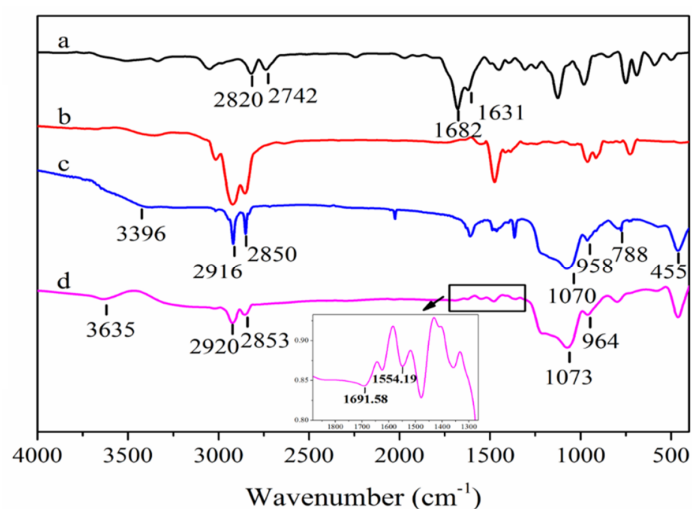


Figure 3. Infrared spectrum (a), CA, (b), Cetyl- trimethyl ammonium bromide (CTAB) surfactant, (c), blank nanoparticle, and (d), SiO_2 -CA.

3.2.2. Crystallography

The XRD spectra of the blank microcapsules and SiO_2 -CA antimicrobial microcapsules are shown in Figure 4. No diffraction peak in the diffraction spectrum was observed while one broad reflection peak (2θ) appeared around $20\sim 25^\circ$, which reflects that the microcapsules prepared by the sol-gel method are composed of amorphous silica, which is completely consistent with the card JCPDS (29-0085). Similar peaks were also found by Matshetshe et al. [26] in the XRD characterization of the silica hollow microspheres prepared. Compared to the XRD curves of the blank microcapsules, the peak

in SiO₂-CA antimicrobial microcapsules reduced and the angle shifted to the left. This “Bang”-like peak in the high angle range indicates that CA has successfully encapsulated. Similar results were also reported by Qu et al. [37].

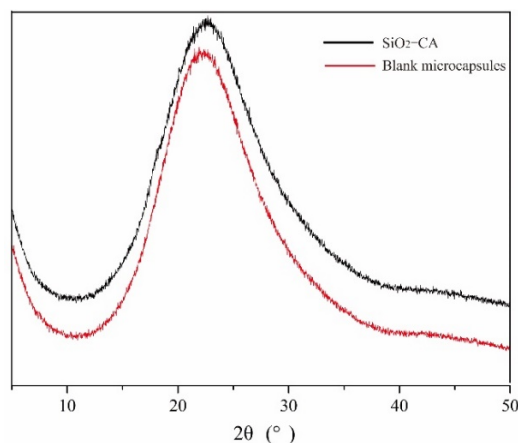


Figure 4. X-ray Diffractometer (XRD) patterns of SiO₂-CA microcapsules and blank microcapsules.

3.2.3. Surface Morphology

The morphologies of four microcapsule samples are shown in Figure 5A. With the increase of CA concentrations, the particle size increased. This was probably due the filling the irregular pores of blank SiO₂. SiO₂-CA microcapsules were regular spheres and the particle size was in the range of 450–700 nm. Similar results were also reported by Qu et al. [37]. Figure 5A shows a transmission electron microscopy (TEM) image of SiO₂-CA microcapsules where it exhibited a “shell-core” structure with a silica shell thickness of approximately 40 nm. As expected, the manner and speed at which TEOS was added, affected the nucleation process. This is because the silanol polycondensation reaction is a process in which nuclear formation and growth are synchronized, leading to mixed growth between grains and consequently resulting in a smaller crystal volume.

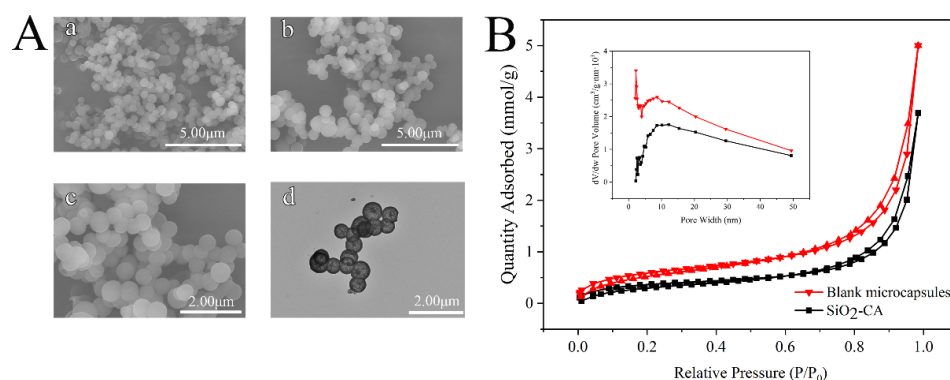


Figure 5. (A): Field-Emission Scanning Electron Microscope (FE-SEM) and transmission electron microscopy (TEM) images of silica microcapsules, (a), Blank microcapsules $\times 10$ K, (b), SiO₂-CA $\times 10$ K, (c), SiO₂-CA $\times 20$ K, (d), TEM image of SiO₂-CA; (B): Nitrogen adsorption-desorption isotherm of microcapsules (within Pore size distribution of microcapsules).

Figure 5B displays the nitrogen adsorption-desorption isotherms of blank and SiO₂-CA microcapsules. According to the IUPAC classification, the curve obtained was type IV isotherm while the hysteresis loop was a H3-type loop, which is a typical feature of mesoporous materials [38,39]. Based on the Barrett–Joyner–Halenda (BJH) theory, the specific surface areas of blank and SiO₂-CA microcapsules were 49.42 and 29.39 m²/g, respectively [25]. As illustrated, the overall adsorption

capacity of SiO₂-CA microcapsules was lower than that of blank microcapsules, indicating that some CA molecules filled and accumulated the mesopores in silica with an increase in pressure, which is consistent with the results reported by Wu [40]. It can be seen from the pore-size distribution curve that both the samples show peaks at approximately 2, 3, and 8 nm, which confirms that the silica microcapsules are mesoporous [41]. The appearance of similar peaks in different samples indicates that the addition of CA does not affect the pore structure of the silica shell, but it affects the pore volume. The pore volume of blank microcapsules was significantly larger than that of SiO₂-CA microcapsules, which might be due to partial CA degradation during sample processing, and the degradation products reduced the pore volume.

3.3. Sustained-Release Performance Analysis

Figure 6A shows the sustained release profiles of SiO₂-CA microcapsules at different temperatures (40, 23, and 4 °C). Active-agent released over 15 days which was divided into three stages, rapid release from 0–18 h, slow-release from 19 h to equilibrium, and the final plateau (complete release on the 3rd d at 40 °C, the 7th d at 25 °C and the 9th d at 4 °C). It was observed that the amount of CA release expands with increasing temperature. These results were consistent with the work of Ke et al. [42]. More than 70% of CA was released after 18 h at 40 °C. The rapid release of CA at high temperatures was theorized to be due to the desorption of CA from the surface of the microcapsules and the outer layer of the silica network. On the other hand, the release rates of CA at 18 h and 9 d were 32.35% and 56.08% respectively at 4 °C. The sustained release was mainly due to the release of CA from the bulk of the silica network. The microcapsule structure effectively prolongs the release and diffusion of CA, and with the accumulation of CA release, the release rate gradually slows down. Ueoka and Mohammadi et al. [32,43] have also noticed the effect of temperature and stated that high temperature can control the release of antibacterial agents and low temperature can delay its effect.

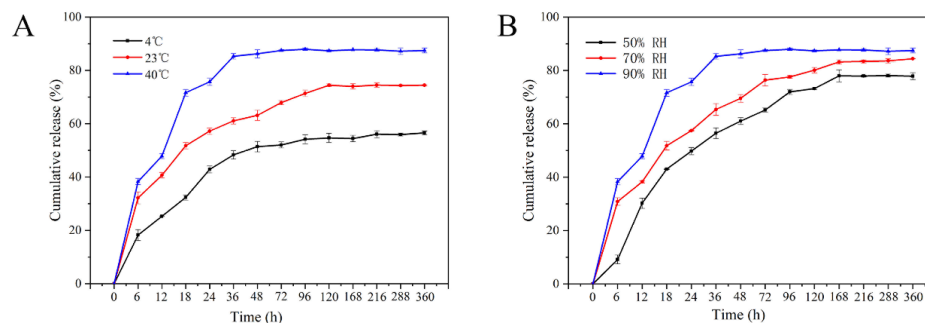


Figure 6. (A): Release curve of microcapsules at different temperatures (4, 23, and 40 °C); (B): Release curve of SiO₂-CA microcapsules under different humidity conditions (50%, 70%, and 90% relative humidity (RH)).

Figure 6B shows the sustained release profile of SiO₂-CA microcapsules at different humidity levels (90%, 70%, and 50% RH). Similar to the effect of temperature, the release of microcapsules within 15 days was classified into three stages. In addition, SiO₂-CA microcapsules have different equilibrium points at different humidity conditions. CA release reaches equilibrium after 3 days at 90% RH. At 70% and 50% RH, CA release reaches equilibrium on the 7th and 9th days, respectively, which means that SiO₂-CA microcapsules exhibit a longer release time under low humidity conditions. Balaguer et al. and Herrera et al. found similar results control release of CA in gliadin films [44,45]. The effect of humidity on the release performance of SiO₂-CA microcapsules might be explained by the presence of a large number of hydroxyl groups on the surfaces of SiO₂-CA microcapsules. In high humid environments, water vapor enters the interior of SiO₂-CA microcapsules, owing to which internally entrapped CA leaches out rapidly.

The first-order release kinetic model was adopted to study the release kinetics of microcapsules. The characteristic of the first-order kinetic model is that the release rate of the antibacterial agent is proportional to the release time, which is suitable for the study of the release law of most polymers [46]. The results are shown in Table 1. R^2 indicated that the sustained release process of CA in SiO₂-CA microcapsules follows the first-order kinetic model, and the effect of humidity was more significant than temperature. In addition, the zero-order kinetic model [47], Higuchi kinetic model [48], and Korsmeyer–Peppas model [48] were also used to simulate the release behavior of the microcapsules, but R^2 indicated that the simulation results do not match. Specific relevant research results are included in Table S1.

Table 1. Fitting results for first-order model of SiO₂-CA microcapsules.

Equation Model	Release Condition	Fitting Equation	R ²	
$\ln\left(1 - \frac{M_t}{M_{\infty}}\right) = -k_1 t$	90%RH	4 °C	$Q = 55.1637 (1 \times 10^{-0.0555}t)$	0.9835
		23 °C	$Q = 74.1331 (1 \times 10^{-0.0618}t)$	0.9438
		40 °C	$Q = 87.7758 (1 \times 10^{-0.08}t)$	0.9751
	40 °C	50%RH	$Q = 75.7937 (1 \times 10^{-0.0465}t)$	0.9867
		70%RH	$Q = 84.2127 (1 \times 10^{-0.0480}t)$	0.9934
		90%RH	$Q = 87.7758 (1 \times 10^{-0.08}t)$	0.9751

3.4. Antibacterial Activity Analysis

Table 2 shows the in-vitro antibacterial efficacy of SiO₂-CA microcapsules against *Listeria monocytogenes* and *Escherichia coli*. As expected, the antibacterial activity of the pure PBAT film against the two bacteria was not detected, and its growth was the same as the blank or negative control. However, the film containing microcapsules performed superior antibacterial activity against the two tested bacteria, which largely depended on the concentration of the microcapsules and the type of bacteria. The antibacterial effect of CA was probably due the presence of nucleophilic group (aldehyde group) conjugated to the benzene ring in the CA. The possible mechanism is that the hydrophilic groups on the surface of the bacteria can adsorb the aldehyde groups, destroy the polysaccharide structure of the bacterial and fungal cell walls, thus destroying the integrity of the cell film [49,50]. SiO₂-CA microcapsules exhibited distinctive antibacterial activity against *Listeria monocytogenes*. When the concentration of SiO₂-CA microcapsules is in the range of 40–90 mg·mL⁻¹, the diameter of the inhibition zone gradually increased from 12.55 mm to 13.95 mm. However, the antimicrobial ring with a diameter of 11.01 mm appeared at an 80 mg/concentration of SiO₂-CA microcapsules against *E. coli* specie. This implies that the antimicrobial effect of microcapsules on *E. coli* was not as satisfactory as that on the *Listeria monocytogenes* species. Similar results were reported by Shankar et al. [2] in grapefruit seed extract. Corrales et al. [51] stated that the lipid constituent in the cell wall of Gram-negative bacteria is a hinderance for the active ingredients extracted from plants to enter in to the cytoplasm and therefore the inhibitory effect of *E. coli* was slightly worse.

Table 2. Antibacterial effect of microcapsules on *Listeria monocytogenes* and *E. coli*.

Concentration (mg·mL ⁻¹)	Inhibition Zone Diameter (mm)	
	<i>Listeria Monocytogenes</i>	<i>E. coli</i>
Blank control	–	–
Negative control	–	–
40	12.55	–
50	12.70	–
60	12.74	–
70	12.89	–
80	13.26	11.08
90	13.95	11.99

“–” means no zone of inhibition.

3.5. Modification Effect of Microcapsule on Films

3.5.1. Physical Properties of Films

As shown in Figure 7A, the mechanical properties of the films first increased and then decreased with increasing the concentration of microcapsules in PBAT films. As the content of SiO₂-CA microcapsules increased to 2.5%, the tensile strength of the PSC composite film increased to 13.6 MPa, which increased by 26.98% compared to the pure PBAT film. It shows that the additions play an important role in enhancing the tensile strength of the film. However, the tensile strength of the PSC-4.5% film sharply decreased, reduced by 32.16% compared with PSC-2.5% film, which was similar to previous reports [18,52]. Unlike tensile strength, the elongation at break of the film continued to decrease, from 786.0% of pure PBAT to 479.6% of PSC-4.5% film, with a decrease of 38.98%. This indicates that an appropriate amount of SiO₂-CA uniformly dispersed in the matrix material which were also found in the results of the electron microscope. At the same time, the number of PBAT crystal nuclei increased due to heterogeneous nucleation. However, further addition of microcapsules had disturbed the original intermolecular arrangement, resulting in a poor dispersion of microcapsules in the PBAT matrix, probably causing stress concentration, and leading to a decrease in tensile strength and elongation at break. Similar results regarding the effect of nanofillers on the mechanical properties of thin films have also been reported by Bastarrachea et al. [18].

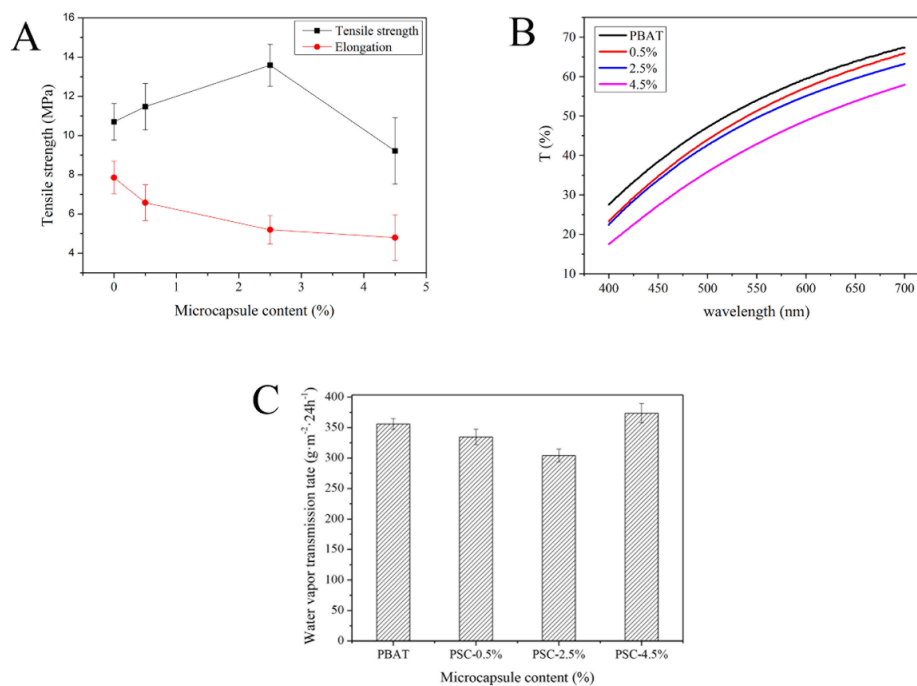


Figure 7. (A): Tensile strength and elongation at break of poly (butyleneadipate-co-terephthalate) (PBAT) and PBAT/SiO₂-CA (PSC) films; (B): water vapor transmission rate (WVTR) of PBAT and PSC films; (C): transmittance of PBAT and PSC films.

The light transmittance of the film is shown in Figure 7B. The transmittance of the pure PBAT film was 67.33%; however, it gradually decreased during the process of adding SiO₂-CA microcapsules, which might be explained that the prepared microcapsules are light yellow powder, resulting in the color of the film-forming fluid gradually changed to yellow with the increase of the added amount. Similar results were reported by Shankar et al. [22].

The WVTR of the films are described in Figure 7C. The WVTR of the pure PBAT film was 355.94 g·m⁻²·24 h⁻¹, while in PSC-2.5%, the value dropped to 303.95 g·m⁻²·24 h⁻¹. Ke et al. [44] also observed similar results. The possible reason should be the distribution of SiO₂-CA microcapsules

in the film which prolongs the movement path of water vapor molecules, increased the difficulty of water vapor passing through the film, and thus improved the moisture resistance [53]. Another reason could be the heterogeneous nucleation of SiO₂-CA antimicrobial microcapsules, which increased the crystallinity of the polymer [54]. The effect of heterogeneous nucleation of microcapsules was also confirmed by the DSC characterization results. However, when the added amount increased to 4.5%, WVTR increased to 373.53 g·m⁻²·24 h⁻¹. Extra microcapsules will cause to merge in the film matrix, which may cause larger “micropores” inside the polymer, thereby promoting the concentrated transmission of water vapor at this location and weakening the barrier properties of water vapor [55].

3.5.2. Thermodynamic Properties of Films

The DSC non-isothermal crystallization curve of the composite film is shown in Figure 8A, and the relative parameters are listed in Table 3. Addition of SiO₂-CA antimicrobial microcapsules had changed the crystallization behavior of PBAT. Adding 0.5% microcapsules increased the crystallization temperature (T_c) of the PSC composite antibacterial film from 61.54 to 66.44 °C, and the initial crystallization temperature (T_{onset}) also increased from 92.91 °C to 94.20 °C. With the addition of microcapsules up to 2.5%, the T_c of PSC composite antibacterial film reached to 70.25 °C, compared with pure PBAT (8.71 °C), and its T_{onset} also increased to 94.65 °C. The reduction of supercooling in the PSC film system was reflected in the increase in crystallization temperature and initial crystallization temperature, which indicates that the SiO₂-CA antimicrobial microcapsules played a heterogeneous nucleation role [31,56]. The second heating curve (Figure 8B) shows that the melting temperature (T_m) of PBAT was 123.13 °C, and the crystallinity (X_c) is 11.12%. After adding SiO₂-CA antimicrobial microcapsules to PBAT, the melting peak of the PSC composite film moved to a high-temperature direction, T_m increased, and the crystallinity also increased slightly. This was mainly because SiO₂-CA microcapsules acted as heterogeneous nucleating agents. Increasing the thickness of the wafer and the X_c of the PBAT polymer turned it difficult to recrystallize the crystal [57]. However, when the SiO₂-CA content reached to 4.5%, the T_m of the PSC composite antibacterial film decreased, which might be due to the agglomeration of a large number of SiO₂-CA microcapsules or the reduction of the heterogeneous nucleation degree, which was related to the decrease in crystallinity.

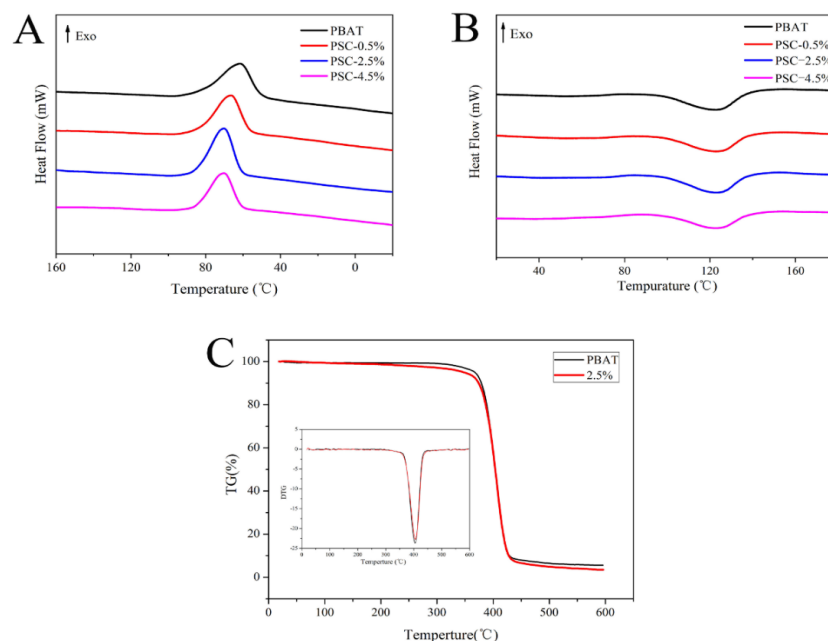


Figure 8. (A): Differential scanning calorimetry (DSC) non-isothermal crystallization curve of PBAT and PSC films; (B): DSC melting curve of PBAT and PSC films; (C): Thermogravimetric curve of films (within derivative thermogravimetric curve).

Table 3. DSC parameters of PBAT and PSC films.

Sample	T _{onset} (°C)	T _c (°C)	T _m (°C)	X _c (%)
PBAT film	92.91	61.54	123.13	11.12
PSC-0.5% film	94.20	66.44	124.06	11.22
PSC-2.5% film	94.65	70.25	123.49	11.67
PSC-4.5% film	92.67	70.21	123.28	10.10

The thermal stability of the antibacterial film was evaluated by thermogravimetric analysis (TG). The following experiment was conducted on the PSC-2.5 films, which was confirmed to perform better. Figure 8C shows the TG curve and derivative thermogravimetry (DTG) of pure PBAT film and composite film of 2.5% SiO₂-CA microcapsules, respectively. As can be seen, the PBAT film, and the PSC-2.5% antibacterial film are both one-step degradation processes, which remain stable up to 383 °C. Compared to the pure PBAT film, the thermal stability of the PSC- 2.5% antibacterial film was slightly worse, which could be caused by the instability of CA inside the microcapsules at high temperature [58]. In the range of 360–430 °C, the film quality loss reached the maximum, the mass losses of PBAT film and PSC-2.5% antibacterial film were 91.97% and 90.79%, respectively. It was observed that the two degradation curves were very similar, which were attributed to the thermal stability of the additives, and the protection provided for essential oil components by microcapsule shell. However, considering the small contribution of the extract to the total mass of the material, it only means that a small number of microcapsules hardly affect the thermal stability of the film [59]. Both the PBAT film and the composite film had two weightlessness stages, namely, a slow decomposition stage and a severe decomposition stage. The presence of clear endothermic peak at the critical point of the two stages, and the fastest weight loss at 404.5 and 405.9 °C, with a difference of 1.4 °C confirmed the good compatibility of microcapsules and films [45].

3.5.3. Surface Morphology of Films

Figure 9 shows the cross-section of the films. The pure PBAT film in picture a has a smooth cross-section without impurities. In Figure 9b, the microcapsules are distributed in partial regions due to the insufficient amount, while in image c, the microcapsules are evenly distributed throughout the cross-section. This demonstrate that the 2.5% SiO₂-CA microcapsules have good compatibility with the PBAT matrix. In Figure 9d, agglomeration can be observed on the surface of the film, which could cause stress concentration in the film and increases the gap between the two phases [31]. This shows that the dispersibility of microcapsules had a certain effect on physical properties.

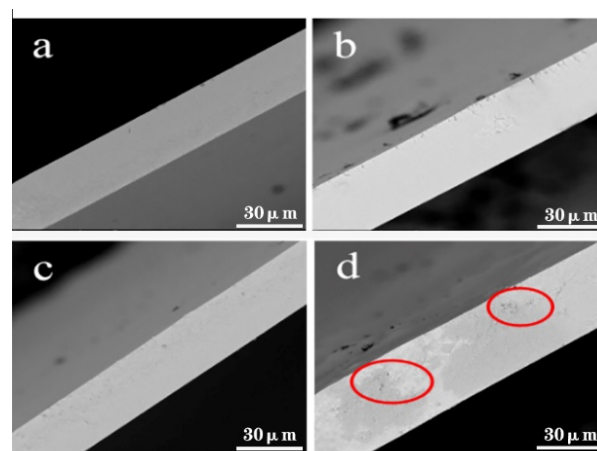


Figure 9. Cross-sectional morphology of films; (a), PBAT film, (b), PSC-0.5%, (c), PSC-2.5%, (d), PSC-4.5%.

3.5.4. Antibacterial Properties of Films

Figure 10 shows the antibacterial effect of the film. The colonies of the blank control flourished, but the bacterial growth on the surface of the antibacterial film was significantly ($p < 0.05$) reduced. This indicates that the PSC composite film has a good antibacterial effect on *E. coli* and *Listeria monocytogenes*. The antibacterial activity of the developed film increased with the increasing microcapsule content, and the antibacterial rate of PSC-2.5 film reached to 100%. It shows that a small number of antimicrobial microcapsules are not enough to achieve a complete antibacterial effect. The antimicrobial efficiency of PSC-0.5 film to *E. coli* and *Listeria monocytogenes* were 95.32% and 95.76%, respectively. It was confirmed that the antimicrobial microcapsules were successfully incorporated into the PBAT films, which effectively prevented the growth of the two tested bacteria.

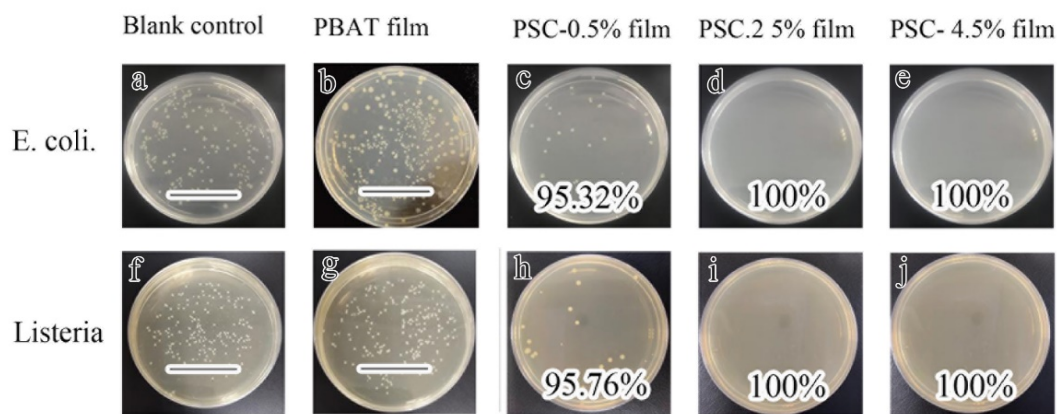


Figure 10. Image (a–e) were the *E. coli* antibacterial results of films; Image (f–j) were *Listeria monocytogenes* antibacterial results of films (“–” means no zone of inhibition).

4. Conclusions

We developed a system for preparing sustained-release antimicrobial microcapsules and their application on PBAT films. By controlling the content of CA, nano-sized steady SiO₂-CA microcapsules with high encapsulation efficiency were obtained. Wall material of SiO₂ prolonged the release time of CA and thus produced a long-lasting effect of antibacterial substances. The first-order kinetic drug release model was suitable for the release behavior of CA. Incorporation of microcapsules into the PBAT film effectively inhibited the growth of *E. coli* and *Listeria monocytogenes*. This work provides a reference for further development of stimuli-responsive packaging by taking advantage of the dependence of microcapsule release behavior on temperature and humidity. However, further research is needed to determine the antimicrobial activity of the developed microcapsules and composite films against other microorganisms and their potential role as food packaging materials.

Supplementary Materials: The following are available online at <http://www.mdpi.com/2227-9717/8/8/897/s1>, The specific fitting results of zero-order release kinetic model, first-order kinetic model, Higuchi kinetic model, and Korsmeyer–Peppas model of microcapsules are shown in Table S1: Fitting results for release kinetic models of SiO₂-CA microcapsules.

Author Contributions: Conceptualization, C.H.; methodology, Y.X.; software, H.H.; investigation, X.D.; resources, C.H.; data curation, Y.X.; writing—original draft preparation, Y.X.; writing—review and editing, Y.X., M.R.K. and Y.Z.; supervision, C.H.; funding acquisition, S.W. All authors have read and agreed to the current version of the manuscript for publication.

Funding: This work was supported by the National Natural Science Foundation of China [215607003] and Guangxi Natural Science Foundation of China (2019JJD120012).

Acknowledgments: The authors wish to express their gratitude to the Large Instrument Platform at the Institute of Light Industry and Food Engineering, Guangxi University, China.

Conflicts of Interest: The authors declare no conflict of interest.

References

1. Elgayyar, M.; Draughon, F.A.; Golden, D.A.; Mount, J.R. Antimicrobial activity of essential oils from plants against selected pathogenic and saprophytic microorganisms. *J. Food Prot.* **2001**, *64*, 1019–1024. [[CrossRef](#)]
2. Shankar, S.; Rhim, J.W. Effect of types of zinc oxide nanoparticles on structural, mechanical and antibacterial properties of poly(lactide)/poly(butylene adipate-co-terephthalate) composite films. *Food Packag. Shelf Life* **2019**, *21*, 100327. [[CrossRef](#)]
3. Shiroodi, S.G.; Nesaei, S.; Ovissipour, M.; Al-Qadiri, H.M.; Rasco, B.; Sablani, S. Biodegradable Polymeric Films Incorporated with Nisin: Characterization and Efficiency against *Listeria monocytogenes*. *Food Bioprocess Technol.* **2016**, *9*, 958–969. [[CrossRef](#)]
4. Khaneghah, A.M.; Hashemi, S.M.B.; Limbo, S. Antimicrobial agents and packaging systems in antimicrobial active food packaging: An overview of approaches and interactions. *Food Bioprod. Process.* **2018**, *111*, 1–19. [[CrossRef](#)]
5. Cardoso, L.G.; Santos, J.C.P.; Camilloto, G.P.; Miranda, A.L.; Druzian, J.I.; Guimardes, A.G. Development of active films poly (butylene adipate co-terephthalate)—PBAT incorporated with oregano essential oil and application in fish fillet preservation. *Ind. Crops Prod.* **2017**, *108*, 388–397. [[CrossRef](#)]
6. Friedman, M.; Henika, P.R.; Mandrell, R.E. Bactericidal activities of plant essential oils and some of their isolated constituents against *Campylobacter jejuni*, *Escherichia coli*, *Listeria monocytogenes*, and *Salmonella enterica*. *J. Food Prot.* **2002**, *65*, 1545–1560. [[CrossRef](#)] [[PubMed](#)]
7. Ghani, S.; Barzegar, H.; Noshad, M.; Hojjati, M. The preparation, characterization and in vitro application evaluation of soluble soybean polysaccharide films incorporated with cinnamon essential oil nanoemulsions. *Int. J. Biol. Macromol.* **2018**, *112*, 197–202. [[CrossRef](#)] [[PubMed](#)]
8. Shreaz, S.; Wani, W.A.; Behbehani, J.M.; Raja, V.; Irshad, M.; Karched, M.; Ali, I.; Siddiqi, W.A.; Hun, L.T. Cinnamaldehyde and its derivatives, a novel class of antifungal agents. *Fitoterapia* **2016**, *112*, 116–131. [[CrossRef](#)] [[PubMed](#)]
9. Uzunlu, S.; Niranjana, K. Laboratory antimicrobial activity of cinnamaldehyde and pomegranate-based polycaprolactone films. *J. Appl. Polym. Sci.* **2017**, *134*, 45347. [[CrossRef](#)]
10. Munhuweyi, K.; Caleb, O.J.; van Reenen, A.J.; Opara, U.L. Physical and antifungal properties of beta-cyclodextrin microcapsules and nanofibre films containing cinnamon and oregano essential oils. *Lwt-Food Sci. Technol.* **2018**, *87*, 413–422. [[CrossRef](#)]
11. Lisuzzo, L.; Cavallaro, G.; Milioto, S.; Lazzara, G. Layered composite based on halloysite and natural polymers: A carrier for the pH controlled release of drugs. *New J. Chem.* **2019**, *43*, 10887–10893. [[CrossRef](#)]
12. Guo, X.Z.; Zhang, Q.L.; Ding, X.G.; Shen, Q.H.; Wu, C.C.; Zhang, L.J.; Yang, H. Synthesis and application of several sol-gel-derived materials via sol-gel process combining with other technologies: A review. *J. Sol-Gel Sci. Technol.* **2016**, *79*, 328–358. [[CrossRef](#)]
13. Vallet-Regi, M.; Ramila, A.; del Real, R.P.; Perez-Pariente, J. A new property of MCM-41: Drug delivery system. *Chem. Mater.* **2001**, *13*, 308–311. [[CrossRef](#)]
14. Xue, J.M.; Shi, M. PLGA/mesoporous silica hybrid structure for controlled drug release. *J. Control Release* **2004**, *98*, 209–217. [[CrossRef](#)] [[PubMed](#)]
15. Meaney, S.P.; Tabor, R.F.; Follink, B. Synthesis and characterisation of robust emulsion-templated silica microcapsules. *J. Colloid Interface Sci.* **2017**, *505*, 664–672. [[CrossRef](#)]
16. Wells, C.; Vollin-Bringel, O.; Fiegel, V.; Harlepp, S.; Van der Schueren, B.; Begin-Colin, S.; Begin, D.; Mertz, D. Engineering of Mesoporous Silica Coated Carbon-Based Materials Optimized for an Ultrahigh Doxorubicin Payload and a Drug Release Activated by pH, T, and NIR-light. *Adv. Funct. Mater.* **2018**, *28*, 1706996. [[CrossRef](#)]
17. Ji, Q.M.; Qiao, X.; Liu, X.B.; Jia, H.B.; Yu, J.S.; Ariga, K. Enhanced Adsorption Selectivity of Aromatic Vapors in Carbon Capsule Film by Control of Surface Surfactants on Carbon Capsule. *B Chem. Soc. Jpn.* **2018**, *91*, 391–397. [[CrossRef](#)]
18. Bastarrachea, L.; Dhawan, S.; Sablani, S.S.; Mah, J.H.; Kang, D.H.; Zhang, J.W.; Tang, J. Biodegradable Poly(butylene adipate-co-terephthalate) Films Incorporated with Nisin: Characterization and Effectiveness against *Listeria monocytogenes*. *Int. J. Food Sci. Nutr.* **2010**, *75*, E215–E224. [[CrossRef](#)]

19. Ferreira, F.V.; Cividanes, L.S.; Gouveia, R.F.; Lona, L.M.F. An overview on properties and applications of poly(butylene adipate-co-terephthalate)-PBAT based composites. *Polym. Eng. Sci.* **2019**, *59*, E7–E15. [[CrossRef](#)]
20. Li, W.L.; Coffin, D.R.; Jin, T.Z.; Latona, N.; Liu, C.K.; Liu, B.; Zhang, J.W.; Liu, L.S. Biodegradable composites from polyester and sugar beet pulp with antimicrobial coating for food packaging. *J. Appl. Polym. Sci.* **2012**, *126*, E361–E372. [[CrossRef](#)]
21. Nofar, M.; Tabatabaei, A.; Sojoudiasli, H.; Park, C.B.; Carreau, P.J.; Heuzey, M.C.; Kamal, M.R. Mechanical and bead foaming behavior of PLA-PBAT and PLA-PBSA blends with different morphologies. *Eur. Polym. J.* **2017**, *90*, 231–244. [[CrossRef](#)]
22. Shankar, S.; Rhim, J.W. Preparation of antibacterial poly(lactide)/poly(butylene adipate-co-terephthalate) composite films incorporated with grapefruit seed extract. *Int. J. Biol. Macromol.* **2018**, *120*, 846–8524. [[CrossRef](#)]
23. Thiyagu, T.T.; Rajeswari, N. Effect of nanosilica and neem tree oil on antimicrobial, thermal, mechanical and electrical insulate of biodegradable composite film. *Mater. Res. Express* **2019**, *6*, 095410. [[CrossRef](#)]
24. Alarcon-Moyano, J.K.; Bustos, R.O.; Herrera, M.L.; Matiacevich, S.B. Alginate edible films containing microencapsulated lemongrass oil or citral: Effect of encapsulating agent and storage time on physical and antimicrobial properties. *J. Food Sci. Technol.* **2017**, *54*, 2878–2889. [[CrossRef](#)]
25. Barrett, E.P.; Joyner, L.G.; Halenda, P.P. The determination of pore volume and area distributions in porous substances. I. Computations from nitrogen isotherms. *J. Am. Chem. Soc.* **1951**, *73*, 373–380. [[CrossRef](#)]
26. Matshetshe, K.I.; Parani, S.; Manki, S.M.; Oluwafemi, O.S. Preparation, characterization and in vitro release study of beta-cyclodextrin/chitosan nanoparticles loaded Cinnamomum zeylanicum essential oil. *Int. J. Biol. Macromol.* **2018**, *118*, 676–682. [[CrossRef](#)]
27. Wu, J.L.; Liu, H.; Ge, S.Y.; Wang, S.; Qin, Z.Q.; Chen, L.; Zheng, Q.H.; Liu, Q.Y.; Zhang, Q.Q. The preparation, characterization, antimicrobial stability and in vitro release evaluation of fish gelatin films incorporated with cinnamon essential oil nanoliposomes. *Food Hydrocoll.* **2015**, *43*, 427–435. [[CrossRef](#)]
28. Li, J.R.; Zou, J.; Xiao, H.N.; He, B.H.; Hou, X.B.; Qian, L.Y. Preparation of novel nano-sized hydrogel microcapsules via layer-by-layer assembly as delivery vehicles for drugs onto hygiene paper. *Polym.-Basel* **2018**, *10*, 335. [[CrossRef](#)]
29. Moghimi, R.; Aliahmadi, A.; Rafati, H. Antibacterial hydroxypropyl methyl cellulose edible films containing nanoemulsions of thymus daenensis essential oil for food packaging. *Carbohydr. Polym.* **2017**, *175*, 241–248. [[CrossRef](#)]
30. Zhang, S.C.; Chen, Y.; Campagne, C.; Salaun, F. Influence of a coaxial electrospraying system on the n-hexadecane/polycaprolactone phase change microcapsules properties. *Materials* **2020**, *13*, 2205. [[CrossRef](#)]
31. Huang, C.X.; Zhang, B.D.; Wang, S.F.; Zhang, L.Y.; Wang, J.; Huang, X.Q.; Zhao, Y.; Huang, L.J. Moisture-triggered release of self-produced ClO₂ gas from microcapsule antibacterial film system. *J. Mater. Sci. Technol.* **2018**, *53*, 12704–12717. [[CrossRef](#)]
32. Mohammadi, A.; Hashemi, M.; Hosseini, S.M. Chitosan nanoparticles loaded with Cinnamomum zeylanicum essential oil enhance the shelf life of cucumber during cold storage. *Postharvest Biol. Technol.* **2015**, *110*, 203–213. [[CrossRef](#)]
33. Maftoonazad, N.; Shahamirian, M.; John, D.; Ramaswamy, H. Development and evaluation of antibacterial electrospun pea protein isolate-polyvinyl alcohol nanocomposite mats incorporated with cinnamaldehyde. *Mater. Sci. Eng. C-Mater.* **2019**, *94*, 393–402. [[CrossRef](#)]
34. Wen, P.; Zhu, D.H.; Feng, K.; Liu, F.J.; Lou, W.Y.; Li, N.; Zong, M.H.; Wu, H. Fabrication of electrospun polylactic acid nanofilm incorporating cinnamon essential oil/beta-cyclodextrin inclusion complex for antimicrobial packaging. *Food Chem.* **2016**, *196*, 996–1004. [[CrossRef](#)]
35. Elfeky, S.A.; Mahmoud, S.E.; Youssef, A.F. Applications of CTAB modified magnetic nanoparticles for removal of chromium (VI) from contaminated water. *J. Adv. Res.* **2017**, *8*, 435–443. [[CrossRef](#)]
36. Corradini, C.; Alfieri, I.; Cavazza, A.; Lantano, C.; Lorenzi, A.; Zucchetto, N.; Montenero, A. Antimicrobial films containing lysozyme for active packaging obtained by sol-gel technique. *J. Food Eng.* **2013**, *119*, 580–587. [[CrossRef](#)]
37. Qu, Q.Q.; Wang, H.; He, J.; Su, Z.; Qin, T.F.; Tian, X.Y. Preparation and characterization of temperature-triggered silica microcapsules containing sodium monofluorophosphate with tolerability to extreme pH. *Colloid Surf. A* **2019**, *564*, 152–160. [[CrossRef](#)]

38. Lee, M.H.; Seo, H.S.; Park, H.J. Thyme oil encapsulated in halloysite nanotubes for antimicrobial packaging system. *J. Food Sci.* **2017**, *82*, 922–932. [[CrossRef](#)]
39. Duan, B.; Chang, C.Y.; Ding, B.B.; Cai, J.; Xu, M.; Feng, S.C.; Ren, J.Z.; Shi, X.W.; Du, Y.M.; Zhang, L.N. High strength films with gas-barrier fabricated from chitin solution dissolved at low temperature. *J. Mater. Chem. A* **2013**, *1*, 1867–1874. [[CrossRef](#)]
40. Wu, C.H.; Zhu, Y.; Wu, T.T.; Wang, L.; Yuan, Y.; Chen, J.C.; Hu, Y.Q.; Pang, J. Enhanced functional properties of biopolymer film incorporated with curcumin-loaded mesoporous silica nanoparticles for food packaging. *Food Chem.* **2019**, *288*, 139–145. [[CrossRef](#)]
41. Liu, P.B.; Huang, Y.; Yan, J.; Yang, Y.W.; Zhao, Y. Construction of CuS Nanoflakes Vertically Aligned on Magnetically Decorated Graphene and Their Enhanced Microwave Absorption Properties. *ACS Appl. Mater. Interfaces* **2016**, *8*, 5536–5546. [[CrossRef](#)] [[PubMed](#)]
42. Ke, J.X.; Xiao, L.Y.; Yu, G.X.; Wu, H.J.; Shen, G.H.; Zhang, Z.Q. The study of diffusion kinetics of cinnamaldehyde from corn starch-based film into food simulant and physical properties of antibacterial polymer film. *Int. J. Biol. Macromol.* **2019**, *125*, 642–650. [[CrossRef](#)] [[PubMed](#)]
43. Ueoka, H.; Shimomura, O.; Ueda, K.; Inada, K.; Nomura, R. Release behavior of a polyanion-crosslinked chitosan-poly(N-isopropylacrylamide) gel thermoresponsive material. *J. Appl. Polym. Sci.* **2018**, *135*, 46732. [[CrossRef](#)]
44. Balaguer, M.P.; Borne, M.; Chalier, P.; Gontard, N.; Morel, M.H.; Peyron, S.; Gavara, R.; Hernandez-Munoz, P. Retention and Release of Cinnamaldehyde from Wheat Protein Matrices. *Biomacromolecules* **2013**, *14*, 1493–1502. [[CrossRef](#)]
45. Herrera, A.; Rodriguez, F.J.; Bruna, J.E.; Abarca, R.L.; Galotto, M.J.; Guarda, A.; Mascayano, C.; Sandoval-Yanze, C.; Padula, M.; Felipe, F.R.S. Antifungal and physicochemical properties of inclusion complexes based on beta-cyclodextrin and essential oil derivatives. *Food Res. Int.* **2019**, *121*, 127–135. [[CrossRef](#)]
46. Khaled, S.A.; Burley, J.C.; Alexander, M.R.; Yang, J.; Roberts, C.J. 3D printing of tablets containing multiple drugs with defined release profiles. *Int. J. Pharm.* **2015**, *494*, 643–650. [[CrossRef](#)]
47. Dima, C.; Patrascu, L.; Cantaragiu, A.; Alexe, P.; Dima, S. The kinetics of the swelling process and the release mechanisms of Coriandrum sativum L. essential oil from chitosan/alginate/inulin microcapsules. *Food Chem.* **2016**, *195*, 39–48. [[CrossRef](#)]
48. El-Hamshary, H.; El-Newehy, M.H.; Abdulhameed, M.M.; El-Faham, A.; Elsherbiny, A.S. Evaluation of clay-ionene nanocomposite carriers for controlled drug delivery: Synthesis, in vitro drug release, and kinetics. *Mater. Chem. Phys.* **2019**, *225*, 122–132. [[CrossRef](#)]
49. Helander, I.M.; Alakomi, H.L.; Latva-Kala, K.; Mattila-Sandholm, T.; Pol, I.; Smid, E.J.; Gorris, L.G.M.; von Wright, A. Characterization of the action of selected essential oil components on gram-negative bacteria. *J. Agric. Food Chem.* **1998**, *46*, 3590–3595. [[CrossRef](#)]
50. Sanla-Ead, N.; Jangchud, A.; Chonhenchob, V.; Suppakul, P. Antimicrobial Activity of Cinnamaldehyde and Eugenol and Their Activity after Incorporation into Cellulose-based Packaging Films. *Packag. Technol. Sci.* **2012**, *25*, 7–17. [[CrossRef](#)]
51. Corrales, M.; Han, J.H.; Tauscher, B. Antimicrobial properties of grape seed extracts and their effectiveness after incorporation into pea starch films. *Int. J. Food Sci. Technol.* **2009**, *44*, 425–433. [[CrossRef](#)]
52. Zhang, F.F.; Bai, X.P.; Wei, G.; Wang, G.D.; Shi, Z.Z.; Jun, C. Effects of virgin coconut oil on the physicochemical, morphological and antibacterial properties of potato starch-based biodegradable films. *Int. J. Food Sci. Technol.* **2020**, *55*, 192–200.
53. Chen, G.Q.; Scholes, C.A.; Doherty, C.M.; Hill, A.J.; Qiao, G.G.; Kentish, S.E. The thickness dependence of Matrimid films in water vapor permeation. *Chem. Eng. J.* **2012**, *209*, 301–312. [[CrossRef](#)]
54. Khorasani, M.T.; Joorabloo, A.; Moghaddam, A.; Shamsi, H.; MansooriMoghaddam, Z. Incorporation of ZnO nanoparticles into heparinised polyvinyl alcohol/chitosan hydrogels for wound dressing application. *Int. J. Biol. Macromol.* **2018**, *114*, 1203–1215. [[CrossRef](#)] [[PubMed](#)]
55. Sun, X.X.; Wang, Z.; Kadouh, H.; Zhou, K.Q. The antimicrobial, mechanical, physical and structural properties of chitosan-gallic acid films. *Lwt-Food Sci. Technol.* **2014**, *57*, 83–89. [[CrossRef](#)]
56. Xiao, M.; Gu, S.; Zhu, P.C.; Tang, M.Y.; Zhu, W.D.; Lin, R.X.; Chen, C.L.; Xu, W.C.; Yu, T.; Zhu, J. Tin-Based Perovskite with Improved Coverage and Crystallinity through Tin-Fluoride-Assisted Heterogeneous Nucleation. *Adv. Opt. Mater.* **2018**, *6*, 1700615. [[CrossRef](#)]

57. Olewnik-Kruszkowska, E.; Tarach, I.; Richert, A.; Cichosz, M.; Koter, I.; Nowaczyk, J. Physicochemical and barrier properties of polylactide films including antimicrobial additives. *Mater. Chem. Phys.* **2019**, *230*, 299–307. [[CrossRef](#)]
58. Liu, J.; Li, J.F.; Luo, Z.P.; Liu, Y.B.; Liu, Z.X.; Chen, Z.C.; Ren, Y.F.; Zhu, B.L.; Wang, R.M.; Zhang, Q.Y. A novel multiwalled LiF@GO@SiO₂ microcapsule with high phase change temperature. *Sol. Energy Mater. Sol. Cells* **2019**, *203*, 110188. [[CrossRef](#)]
59. Moreno, M.A.; Orqueda, M.E.; Gomez-Mascaraque, L.G.; Isla, M.I.; Lopez-Rubio, A. Crosslinked electrospun zein-based food packaging coatings containing bioactive chilito fruit extracts. *Food Hydrocoll.* **2019**, *95*, 496–505. [[CrossRef](#)]



© 2020 by the authors. Licensee MDPI, Basel, Switzerland. This article is an open access article distributed under the terms and conditions of the Creative Commons Attribution (CC BY) license (<http://creativecommons.org/licenses/by/4.0/>).